

## A one-dimensional model illustrating virtual-cathode formation in a novel coaxial virtual-cathode oscillator

Geoffrey R. Turner

Citation: [Physics of Plasmas \(1994-present\)](#) **21**, 093104 (2014); doi: 10.1063/1.4895500

View online: <http://dx.doi.org/10.1063/1.4895500>

View Table of Contents: <http://scitation.aip.org/content/aip/journal/pop/21/9?ver=pdfcov>

Published by the [AIP Publishing](#)

---

### Articles you may be interested in

[High power microwave generation from coaxial virtual cathode oscillator using graphite and velvet cathodes](#)  
J. Appl. Phys. **107**, 093301 (2010); 10.1063/1.3399650


[The dependence of vircator oscillation mode on cathode material](#)  
J. Appl. Phys. **105**, 123301 (2009); 10.1063/1.3151863


[A one-dimensional basic oscillator model of the vircator](#)  
Phys. Plasmas **16**, 063104 (2009); 10.1063/1.3155472

[Influence of background gas ionization on oscillations in a virtual cathode with a retarding potential](#)  
Phys. Plasmas **16**, 033106 (2009); 10.1063/1.3080200


[Theory of the virtual cathode oscillator](#)  
Phys. Plasmas **8**, 3781 (2001); 10.1063/1.1382643

---

A collection of five pieces of Pfeiffer Vacuum equipment, including a red turbopump, a silver turbopump, a white turbopump, a red turbopump with a long shaft, and a silver chamber component.

 Vacuum Solutions from a Single Source

- Turbopumps
- Backing pumps
- Leak detectors
- Measurement and analysis equipment
- Chambers and components

**PFEIFFER**  **VACUUM**

# A one-dimensional model illustrating virtual-cathode formation in a novel coaxial virtual-cathode oscillator

Geoffrey R. Turner<sup>a)</sup>

Council for Scientific and Industrial Research, PO Box 395, Pretoria 0001, South Africa

(Received 16 May 2014; accepted 27 August 2014; published online 11 September 2014)

A one-dimensional electrostatic sheet model of a coaxial geometry Virtual Cathode Oscillator (VCO) is presented. The cathode is centrally located and connects to a peripherally located plate electrode to form a resonant cavity, and is thus considered to be a novel design. Charge is modelled as concentric sheets about the cathode whose absolute position and velocity are determined as a function of time by solving the relativistic equations of motion. The model predicts the formation of a virtual cathode between the grid and plate electrodes for the case of a space-charge limited current. Setting the electron reflexing frequency (as a function of the grid potential) comparable with the cavity resonant frequency is predicted to improve the efficiency of microwave emission.

© 2014 AIP Publishing LLC. [<http://dx.doi.org/10.1063/1.4895500>]

## I. INTRODUCTION

The simulation of a relativistic coaxial geometry Virtual Cathode Oscillator (VCO) with centrally located cathode and peripherally located plate is presented. The coaxial VCO (with cathode on the periphery) was originally developed as a source of intense microwaves at Texas Technical University by Crawford *et al.*<sup>1</sup> and Jiang *et al.*<sup>2,3</sup> and is an extension of the planar electrode VCO. The VCO specifically exploits instabilities that result in a space-charge limited electron current in the manner first described by Birdsall and Bridges.<sup>4</sup> Amongst the earliest to exploit this phenomenon for the emission of microwaves were Granatstein *et al.*,<sup>5</sup> Mahaffey *et al.*,<sup>6</sup> Brandt *et al.*,<sup>7</sup> and Phelps<sup>8</sup> in the USA, and Didenko *et al.*<sup>9</sup> and Zherlitsyn *et al.*,<sup>10</sup> in the former Soviet Union. An introduction to the historical, theoretical, and practical aspects of VCO's is provided by Sullivan *et al.*,<sup>11</sup> Thode,<sup>12</sup> Hoerberling and Fazio,<sup>13</sup> and Benford *et al.*<sup>14</sup> More recently, work upon the coaxial VCO has been presented by Choi *et al.*,<sup>15</sup> Luo *et al.*,<sup>16</sup> and Biswas and Kumar.<sup>17,18</sup>

Fig. 1 shows the simulated VCO. The arrangement and purpose of the electrodes are similar to that of the annular reflex klystron described by Wootton *et al.*,<sup>19</sup> with the exception that the cathode of the presented VCO connects to the plate to form a resonant cavity. The electric field within the cavity modulates the velocity of the space-charge traversing the space in the manner described by Fazio *et al.*<sup>20</sup> The cathode is of the explosive emission type similar to that described by Miller,<sup>21</sup> Garate *et al.*,<sup>22</sup> Schiffler *et al.*,<sup>23</sup> and Prohaska and Fisher.<sup>24</sup> Locating the cathode at the centre results in electron emission at lower cathode-grid potential due to higher electric field-strength at the cathode surface (compared with a peripherally located cathode). The grid electrode may comprise porous mesh or foil.

## II. THEORY OF OPERATION

With reference to Fig. 1, electrons (emitted from the cathode) are accelerated towards the grid in the grid-cathode electric field. Electrons that pass through the porous grid are decelerated *en route* to the plate in the opposing grid-plate electric field. Provided the grid-cathode potential is sufficient to result in a space-charge limited current (that is to say the electric field due to the electron flux dominates the field within the cavity) then electrons will accumulate at a distance roughly equivalent to one grid-cathode gap beyond the grid. The virtual cathode depresses the local grid-plate electric field such that subsequent electrons are caused to reflex back and forth about the grid in the manner described by Birdsall and Bridges.<sup>4</sup>

In an effort to maintain the plate and the cathode at the same potential, a conduction current flows in the cavity wall connecting the cathode to the plate. This conduction current lags the space-charge current due to the cavity inductance. Ergo, a time varying Radio Frequency (RF) potential develops between the plate and the cathode. This potential modulates the velocity of space-charge in the cavity by dictating, in part, the electric field between the grid and the plate

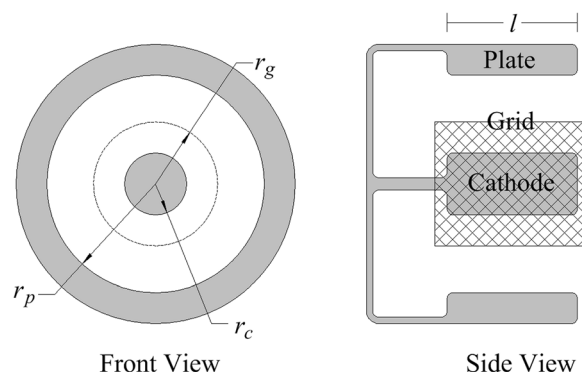


FIG. 1. A coaxial geometry VCO with centrally located cathode (radius  $r_c$ ), peripherally located plate electrode (radius  $r_p$ ) and grid electrode (radius  $r_g$ ). The cathode connects to the plate to form a resonant cavity.

<sup>a)</sup>Electronic mail: gturner@csir.co.za

electrodes (where the remainder is dictated by the space-charge itself). If the cavity dimensions are adjusted such that the cavity resonant frequency  $f_o$  is comparable with the electron reflexing frequency  $f_e$ , then the magnitude of the time varying plate-cathode potential will grow, reinforcing the movement of the space-charge by virtue of the modified cavity field. The RF component of the cavity electric field is extracted as a TM mode by means of a circular waveguide attached to the plate electrode.

In the absence of significant space-charge and for  $r_g/r_c \approx 1$ , the electric field across the grid-cathode gap is a reasonably constant  $E = V_{gc}/d$ , where  $V_{gc}$  is the grid-cathode potential and  $d = r_g - r_c$  is the gap dimension. Equating the electrostatic force  $q_e E$  upon an electron departing the cathode (at time  $t=0$  with velocity  $v_e=0$ ) to the rate of change of electron momentum  $p_e = m_e v_e$  with respect to time, then

$$\frac{dv_e}{dt} = \frac{q_e V_{gc}}{m_e d} \text{ [m/s}^2\text{]}, \quad (1)$$

where  $m_e$  is the electron rest mass ( $9.11 \times 10^{-31}$  kg) and  $q_e$  is the electron charge ( $1.602 \times 10^{-19}$  C).

Equation (1) ignores (for the moment) any relativistic increase in the mass of an electron traversing the gap. Integrating Eq. (1) twice with respect to time while noting that  $r_e(0) = r_c$  and  $v_e = dr_e/dt$ , then

$$r_e = r_c + \frac{q_e V_{gc}}{2m_e d} t^2 \text{ [m]}. \quad (2)$$

Equation (2) determines the radial position  $r_e$  of an electron within the grid-cathode gap as a function of time  $t$ . Setting  $r_e = r_g$  and rearranging Eq. (2), then

$$\tau = d \sqrt{\frac{2m_e}{q_e V_{gc}}} \text{ [s]}, \quad (3)$$

where  $\tau$  is the time taken by an electron to traverse the gap  $d$ .

Since the virtual cathode forms approximately the same distance outside the grid as the grid-cathode gap, then the time required to decelerate an electron to zero velocity *en route* from the grid to the virtual cathode is equivalent to the time  $\tau$  taken to accelerate an electron from the cathode to the grid. Thus, in accordance with Jiang *et al.*<sup>2</sup> and Benford *et al.*,<sup>14</sup> the electron reflexing frequency  $f_e$  is the inverse of the time required to traverse the distance from the cathode to the virtual cathode, and back. Hence,

$$f_e = 1/4\tau = \frac{1}{4d} \sqrt{\frac{q_e V_{gc}}{2m_e}} \text{ [Hz]}. \quad (4)$$

Equation (4) determines, to a first approximation, the frequency of oscillation of electrons *about the grid* for the case where the electric field is assumed uniform either side of the grid. That is to say, the effect upon the electric field due to the electrode profile and space-charge is ignored. As will be shown, the assumption that the electric field is uniform between the cathode, grid, and virtual cathode is not

unrealistic, and thus Eq. (4) may be put to some practical use despite the elementary assumptions employed in its derivation.

### III. A ONE DIMENSIONAL ELECTROSTATIC MODEL

Fig. 2 shows a simple pulsed power supply connected to a VCO. The pulsed power supply comprises capacitor  $C_s$  (charged to voltage  $V_s$ ), equivalent series resistance  $R_s$ , and equivalent series inductance  $L_s$ . Cavity inductance  $L_{pc}$  connects the plate to the cathode, while resistor  $R_{pc}$  loads the cavity. At time  $t=0$ , switch  $S$  is closed, connecting capacitor  $C_s$  to the grid of the VCO, causing currents  $I_p$  and  $I_g$  to flow in the plate and grid electrodes, respectively.

With reference to Fig. 2,

$$\frac{dI_g}{dt} = \frac{V_s - V_{gc} - R_s I_g}{L_s} \text{ [A/s]}, \quad (5)$$

$$\frac{dI_L}{dt} = -\frac{V_{pc}}{L_{pc}} \text{ [A/s]}, \quad (6)$$

$$\frac{dV_s}{dt} = -\frac{I_g}{C_s} \text{ [V/s]}, \quad (7)$$

and

$$I_L = I_p + \frac{V_{pc}}{R_{pc}} \text{ [A]}, \quad (8)$$

where  $V_{pc}$  and  $V_{gc}$  are the plate-cathode and grid-cathode potentials, respectively. Equations (5) through (8) require that  $V_{pc}$  and  $V_{gc}$  be determined by modelling the charge residing both *upon* and *between* the electrodes. Space-charge is assumed uniformly distributed within concentric sheets (of negligible thickness) about the electrodes in a similar manner to the work of Birdsall and Bridges.<sup>4</sup> Each sheet contains charge  $Q_n$ , where the subscript  $n$  is the sheet index. Lines of electric field are radially directed, perpendicular to the sheets. Edge effects are ignored. Applying Gauss's law to the sheets

$$E(r_n) = \frac{1}{2\pi r_n l \epsilon_0} \sum_{i=1}^{i=n} Q_i \text{ [V/m]}, \quad (9)$$

where  $E(r_n)$  is the electric field at the radius  $r_n$  of the  $n$ th sheet,  $l$  is the length of the electrodes, and  $\epsilon_0$  is the electric

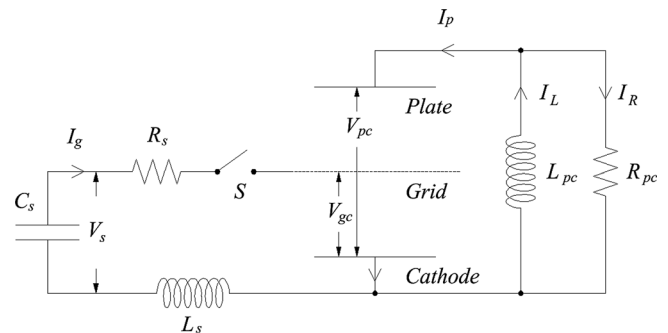


FIG. 2. A pulsed power supply connected to a VCO.

permittivity of free-space ( $8.854 \times 10^{-12}$  F/m). Integrating Eq. (9) across the grid-cathode and plate-cathode gaps,

$$V_{gc} = \frac{1}{2\pi l \epsilon_0} \left[ Q_c \ln\left(\frac{r_g}{r_c}\right) + \sum_{i=1}^{i=n_g} \left( Q_i \ln\left(\frac{r_g}{r_i}\right) \right) \right] \text{ [V]} \quad (10)$$

and

$$V_{pc} = \frac{1}{2\pi l \epsilon_0} \left[ Q_c \ln\left(\frac{r_p}{r_c}\right) + Q_g \ln\left(\frac{r_p}{r_g}\right) + \sum_{i=1}^{i=n_p} \left( Q_i \ln\left(\frac{r_p}{r_i}\right) \right) \right] \text{ [V]}, \quad (11)$$

where  $n_g$  and  $n_p$  denote the last sheet before the grid and plate, respectively. In the absence of space-charge, Eqs. (10) and (11) reduce to

$$V_{gc} = \frac{1}{2\pi l \epsilon_0} \left[ Q_c \ln\left(\frac{r_g}{r_c}\right) \right] \text{ [V]} \quad (12)$$

and

$$V_{pc} = \frac{1}{2\pi l \epsilon_0} \left[ Q_c \ln\left(\frac{r_p}{r_c}\right) + Q_g \ln\left(\frac{r_p}{r_g}\right) \right] \text{ [V]}. \quad (13)$$

Subtracting Eq. (12) from Eq. (13)

$$V_{pg} = \frac{1}{2\pi l \epsilon_0} \left[ (Q_c + Q_g) \ln\left(\frac{r_p}{r_g}\right) \right] \text{ [V]}, \quad (14)$$

where  $V_{pg}$  is the plate-grid potential.

The capacitance of two electrodes separated by a dielectric is defined as the ratio of charge accumulated upon the electrodes to the potential difference measured between the electrodes. Ergo,

$$C_{gc} = \frac{Q_c}{V_{gc}} = \frac{2\pi l \epsilon_0}{\ln(r_g/r_c)} \text{ [F]} \quad (15)$$

is the capacitance of the grid-cathode electrodes, and

$$C_{pg} = \frac{Q_g + Q_c}{V_{pg}} = \frac{2\pi l \epsilon_0}{\ln(r_p/r_g)} \text{ [F]}, \quad (16)$$

is the capacitance of the plate-grid electrodes.

Thus, in the absence of space-charge, Eqs. (10) and (11) return the same result that would be returned if we were to replace the VCO in the circuit of Fig. 2 with two concentric coaxial capacitors. In the presence of space-charge, however, Eqs. (10) and (11) account for both the charge *upon* the electrodes (behaving as capacitors), as well as that *between* the electrodes.

Cathode charge  $Q_c$ , grid charge  $Q_g$ , and plate charge  $Q_p$  are determined by simple conservation of charge flowing into and out of the electrodes

$$Q_c = q_{ce} - \int (I_p + I_g) dt \text{ [C]}, \quad (17)$$

$$Q_g = q_{ge} + \int I_g dt \text{ [C]}, \quad (18)$$

$$Q_p = q_{pe} + \int \left( I_L - \frac{V_{pc}}{R_o} \right) dt \text{ [C]}, \quad (19)$$

where  $q_{ce}$ ,  $q_{ge}$ , and  $q_{pe}$  are the charge of electrons exchanged between cavity and the cathode, grid, and plate electrodes, respectively. It is noteworthy that in the presence of space-charge, Eqs. (17)–(19) do not necessarily sum to zero since the charge entering the cavity (at the cathode) is not necessarily the same as that leaving it (at any other electrode). That is to say, charge may accumulate in the cavity, as is indeed the case when the space-charge current limit is exceeded.

Calculation of charges  $q_{ce}$ ,  $q_{ge}$ , and  $q_{pe}$  requires the movement of charge over the cathode, grid, and plate boundaries be determined, for which the equations of motion must be examined. As before, equating the electrostatic force  $Q_n E$  upon the  $n$ th sheet of charge (due to electric field  $E(r)$  at position  $r = r_n$ ) to the rate of change of momentum of the  $n$ th sheet with respect to time,

$$Q_n E(r_n) = \frac{d}{dt} (m_n v_n) = m_n \frac{dv_n}{dt} + v_n \frac{dm_n}{dt} \text{ [N]}, \quad (20)$$

where  $v_n$  is the radial velocity of the  $n$ th sheet at position  $r = r_n$ ,

$$m_n = \frac{Q_n}{q_e} \times \frac{m_e}{\sqrt{1 - \left(\frac{v_n}{c}\right)^2}} \text{ [kg]} \quad (21)$$

is the relativistic mass of the  $n$ th sheet and  $c$  the speed of light ( $2.998 \times 10^8$  m/s).

Differentiating Eq. (21) with respect to time

$$\frac{dm_n}{dt} = \frac{Q_n m_e v_n}{q_e c^2 \left(1 - \left(\frac{v_n}{c}\right)^2\right)^{\frac{3}{2}}} \times \frac{dv_n}{dt} \text{ [kg/s]}. \quad (22)$$

Substituting Eqs. (21) and (22) into Eq. (20) and rearranging we get

$$\frac{dv_n}{dt} = E(r_n) \frac{q_e}{m_e} \left(1 - \left(\frac{v_n}{c}\right)^2\right)^{\frac{3}{2}} \text{ [m/s}^2\text{]}. \quad (23)$$

Equation (23) determines the relativistic acceleration of the  $n$ th sheet as a function of the electric field  $E(r)$  at position  $r = r_n$  and velocity  $v = v_n$ , where

$$\frac{dr_n}{dt} = v_n \text{ [m/s]}. \quad (24)$$

Equation (23) reduces to the non-relativistic case for  $v_n \ll c$ .

#### IV. NUMERIC SOLUTION

Differential equations (5) through (7), (23), and (24) were numerically integrated following a simple Euler



method. The step-size was typically set no larger than  $2 \times 10^{-13}$  s and data were harvested every 100th iteration in order to compile graphs. Each variable, with the exception of  $V_s$ , was initially set to zero since none of the electrodes, nor the cavity, contain any charge at time  $t=0$ . Equations (10) and (11) were assessed as a function of Eqs. (17) through (19) between iterations. The number of equations that must be solved varies from iteration to iteration as charge is traded between the electrodes and the cavity.

For the purpose of the presented model: Concentric sheets of charge may occupy the same radial position, regardless of velocity. Sheets may overtake each other (due to disparate velocities). Sheets may also carry disparate quantities of charge. All space-charge is of electrons only, while electrode charge may be either negative or positive. Only the cathode may emit charge. If at time  $t+h$  a sheet is determined to have collided with either the cathode or the plate, then the charge of that sheet is added to the charge of the electrode and the sheet deleted from the model. If at time  $t+h$  a sheet is determined to have crossed the grid (regardless of direction), then a fraction of that charge (calculated according to the porosity of the grid) is transferred to the charge of the grid, and the remainder of the sheet allowed to continue onwards. For the purposes of the presented model the grid was considered to have a constant porosity regardless of electron energy, although it is a simple matter to adjust the grid porosity as a function of the kinetic energy of each sheet (as it intersects the grid), as in the work of Biswas and Kumar for their foil anode.<sup>17</sup>

Provided the electric field  $E(r)$  at the surface of the cathode exceeds some predefined value (permitting explosive emission of electrons), then cathode charge  $Q_c$  is transferred to sheet  $n=1$  and the index  $n$  of all other sheets incremented by 1. A minimum electric field strength of 16 kV/cm was chosen for a velvet cathode in accordance with the work of Miller.<sup>21</sup> If desired, an emission current limit may be imposed upon the cathode by limiting the quantity of charge that is transferred to each new sheet per iteration of the model. Newly formed sheets are located on the boundary of the cathode at  $r=r_c$  and allocated an initial velocity of  $v=0$ , ready to be accelerated away during the next iteration of the model.

## V. RESULTS OF CALCULATIONS

Results of the model are presented for a coaxial VCO with dimensions  $r_c=0.03$  m,  $r_g=0.04$  m,  $r_p=0.10$  m, and  $l=0.053$  m. Grid porosity was set to 70%. The pulsed power supply of Fig. 2. comprised  $C_s=100$  nF,  $R_s=0.5$   $\Omega$ , and  $L_s=100$  nH, with  $V_s(0)=50$  kV. The cavity was loaded with  $R_{pc}=50$   $\Omega$  to represent the input impedance of a section of circular waveguide with matched load. If desired, the load may include (in series or parallel) a reactive component to simulate the effect, for example, of an imperfectly matched antenna, thus reflecting power (that would otherwise be radiated) back into the cavity. Substituting the above values into Eqs. (4), (15), and (16), we determine that  $f_e=1.66$  GHz,  $C_{pg}=3.2$  pF, and  $C_{gc}=10.3$  pF.

In a similar manner to Rieke's treatment of the cavity magnetron,<sup>25</sup> the resonant frequency of the cavity (formed between the plate and cathode electrodes) was approximated as

$$f_o = \frac{1}{2\pi\sqrt{L_{pc}C_{pc}}} \text{ [Hz]}, \quad (25)$$

where  $L_{pc}$  is, as before, the cavity inductance, and

$$C_{pc} = \left( \frac{1}{C_{pg}} + \frac{1}{C_{gc}} \right)^{-1} \text{ [F]} \quad (26)$$

is the cavity capacitance.

Substituting the result of Eqs. (15) and (16) into Eq. (26), we determine that  $C_{pc}=2.4$  pF. Setting  $f_o=f_e$  and rearranging Eq. (25), we determine that  $L_{pc}=3.8$  nH. Clearly, if this value cannot be realized within the physical geometry of the device then it is not possible to set the cavity resonant frequency to match the electron reflexing frequency. Alternatively, for a given set of electrodes (of pre-defined dimensions), we may raise or lower the initial voltage to which capacitor  $C_s$  is charged in an effort to match the electron reflexing frequency to the cavity resonant frequency, provided of course the grid-cathode potential remains sufficient to inject a space-charge limited current into the cavity.

Figs. 3(a) through 3(j) show successive phase-space diagrams, calculated using the above values, depicting the velocity of the concentric charge sheets as a function of radial position about the cathode, starting at the cathode and working out towards the plate electrode. A maximum electron velocity of  $\sim 0.4 \times c$  is indicated. It is noteworthy that significantly higher electron velocities are predicted if a non-relativistic model is employed.

Fig. 3(a) shows charge streaming out from the cathode, arriving at the grid at time  $t=1.19$  ns. Fig. 3(b) indicates that by  $t=2.30$  ns, the first charge has arrived at the plate. Compared with the charge which preceded it, charge passing through the grid is now decelerated more rapidly, slowing to zero velocity at a distance roughly equivalent to the cathode-grid gap outside of grid, causing charge to accumulate and the virtual cathode to form. Fig. 3(c) indicates that by  $t=2.67$  ns, charge that had previously decelerated to zero velocity is now accelerated back towards the grid. A bifurcation in the velocity profile, similar to that originally described by Birdsall and Bridges,<sup>4</sup> is now apparent. Fig. 3(d) indicates that the first charge arrives back at the cathode at  $t=2.76$  ns. Charge with three velocities can be discerned between radial positions 0.04 m and 0.05 m. Fig. 3(e) indicates that charge returning to the cathode is decelerated to zero velocity and accelerated back to the grid in Fig. 3(f), where the charge joins new charge emitted from the cathode. Fig. 3(g) shows three separate streams of charge: that emitted from the cathode; that which has traversed the grid; and that due to the bifurcation, returning from part way between the grid and plate. Figs. 3(h) through 3(j) show a further revolution of charge about the grid.

Figs. 4(a) through 4(j) show the calculated electric potential across the cavity, corresponding to the phase-

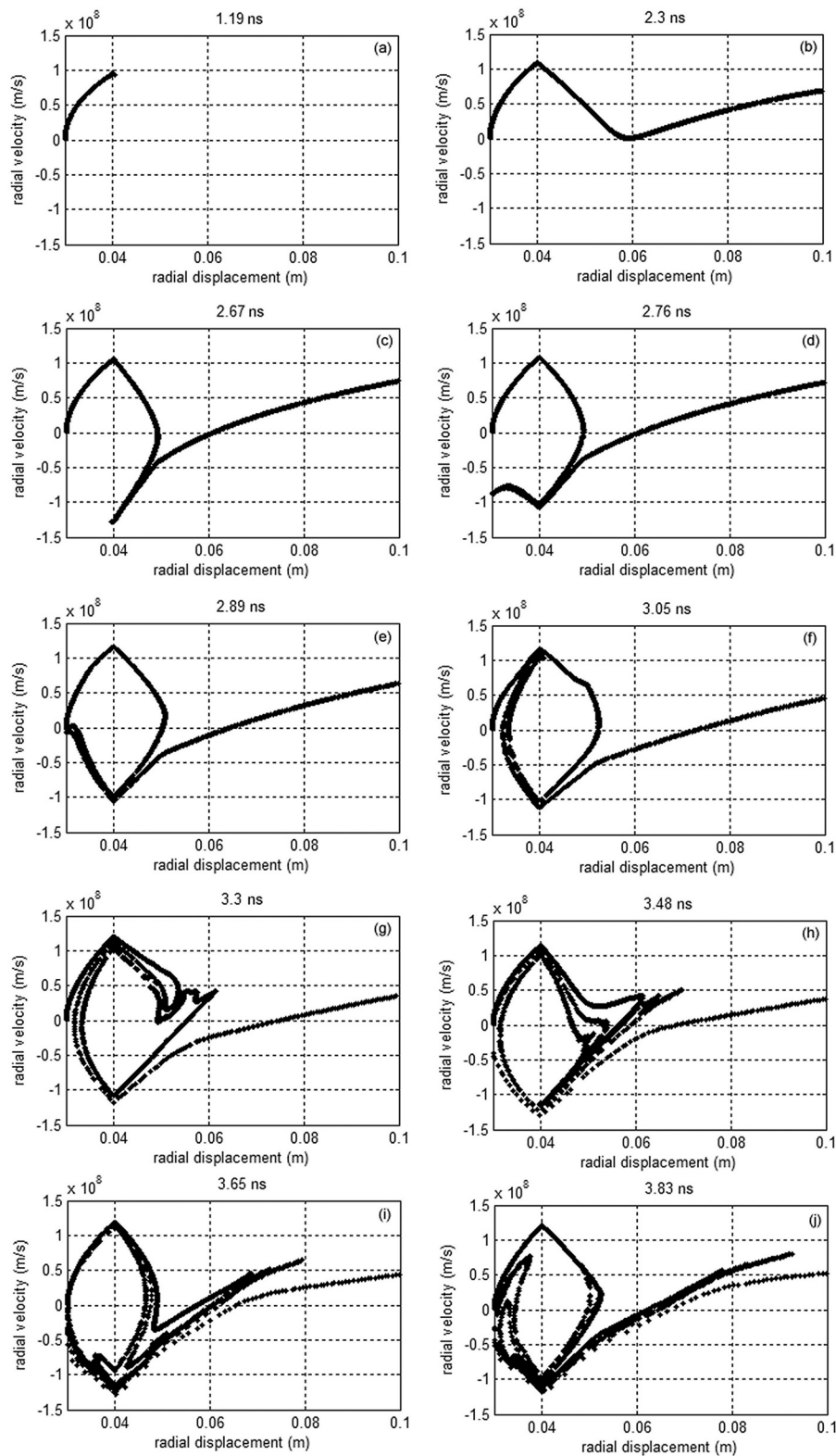


FIG. 3. Successive phase-space diagrams depicting calculated sheet velocity as a function of radial displacement.

space diagrams of Figs. 3(a) through 3(j). The data of Fig. 4 were determined by integrating the calculated electric field (Eq. (9)) from the cathode to the plate. Since the cathode is grounded, the cathode potential is set to 0 V. Fig. 4(a) is similar to that which one would expect for the case of an empty cavity due to the limited flux of electrons entering the space at this early time. Figs. 4(b) through 4(j) clearly illustrate how the electric potential is

modified, compared with that of Fig. 4(a), due to the presence of charge in the cavity. Currents within the inductive connection between the cathode and plate permit the plate potential (indicated at the far right of each graph) to rise and fall as charge traverses the cavity. The grid potential is dictated by the voltage at the output of the pulsed power supply which connects, as per Fig. 2, to the cathode and grid electrodes.

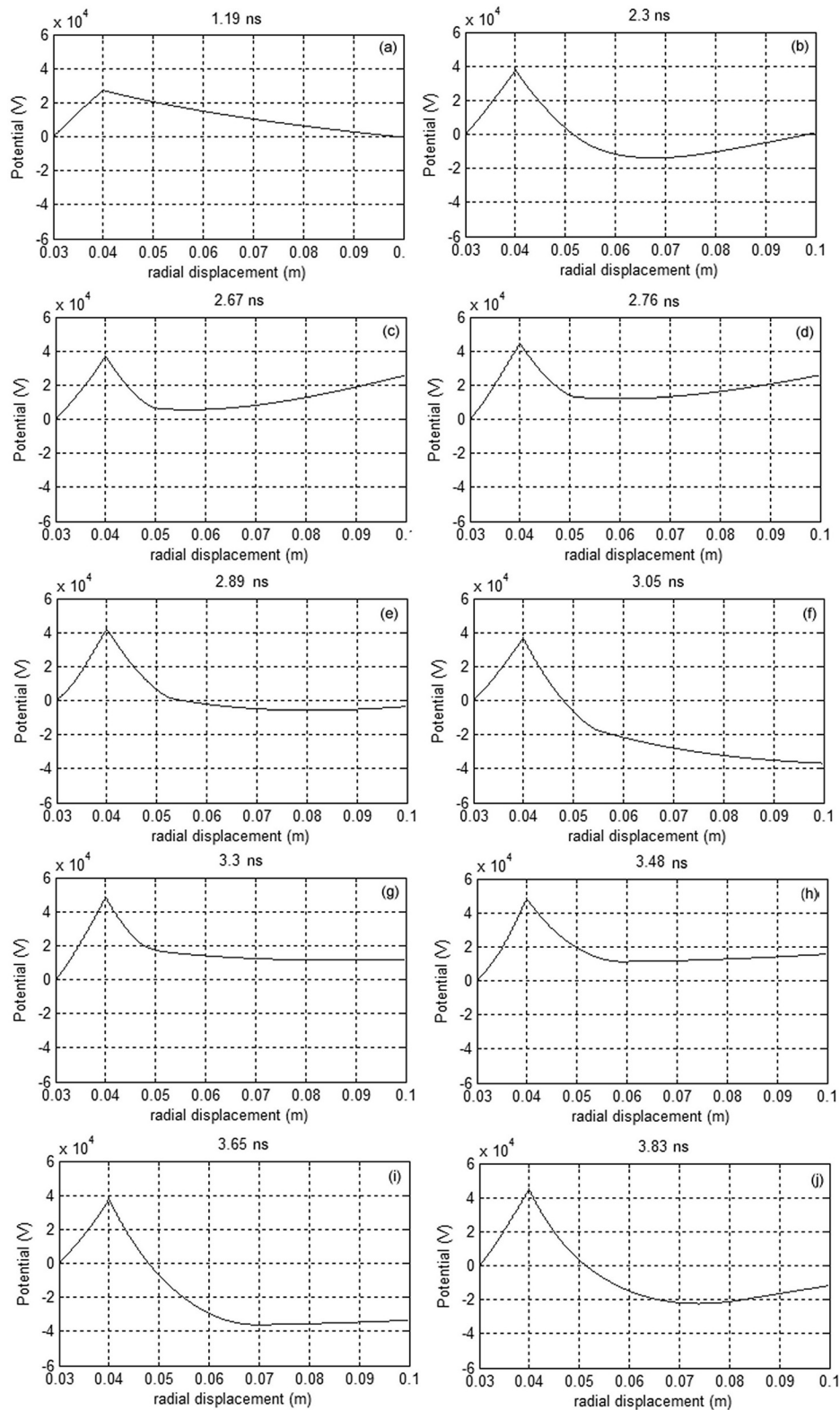


FIG. 4. Successive diagrams depicting calculated electric potential as a function of radial displacement.

The graphs of Fig. 4 indicate that from 2.4 ns onwards, the electric potential outside of the grid is a mirror image of that inside the grid, indicating the presence of the virtual cathode at a distance from the grid roughly equivalent to the cathode-grid gap. Fig. 4 further indicates that the gradient of the electric potential to the immediate inside and outside of the grid (from cathode to virtual cathode) is reasonably constant, indicating that the cathode-grid and grid-virtual-

cathode electric field are likewise reasonably constant, suggesting that Eq. (4) is more useful than might initially be assumed. This was confirmed while inspecting plots of the electric field.

Results of the model, presented in Figs. 3 and 4 are, unsurprisingly, similar to those presented by Sullivan *et al.*,<sup>11</sup> for a planar electrode VCO due to the commonality of the virtual cathode. It is noteworthy that in the case of a

planar VCO with resonant cavity, both the porous anode and the opposite wall of the cavity are maintained at the same mean potential, while in the case of the coaxial VCO presented here, the plate electrode connects to the cathode. Electrons are thus repelled back to the grid not only when the virtual cathode forms, but, in the absence of significant space-charge, *by the plate electrode itself*. In this regard, the presented VCO is similar to the annular reflex klystron oscillator of Wooten *et al.*,<sup>19</sup> which specifically includes a *reflector* electrode designed to return electrons to the cavity. It may, therefore, be more accurate to describe the particular coaxial VCO presented here as a relativistic version of Wooten's annular reflex klystron.

Fig. 5 shows the calculated grid and plate potentials over a period of 25 ns for the case of the electrodes specified above and the cavity inductance  $L_{pc} = 10$  nH, where the cavity inductance was chosen specifically such that  $f_e \neq f_o$  in order that the VCO operates outside of resonance. Fig. 5 indicates the onset of oscillation at a grid potential of  $\sim 40$  kV,  $\sim 2.5$  ns after power is applied to the VCO. The grid is raised to a mean DC potential of 50 kV due to source capacitor  $C_s$ ,  $\sim 5$  ns after switch S is closed. A glance at the plate potential suggests microwave output at multiple frequencies.

An estimation of the power spectral density of the data of Fig. 5 is shown in Fig. 6. The primary (strongest) oscillation at 1.71 GHz correlates well with  $f_e = 1.66$  GHz predicted by Eq. (4). The secondary (next strongest) oscillation at 1.23 GHz correlates well with  $f_o = 1.17$  GHz predicted by Eq. (25). The remaining oscillations are all due to the intermodulation of the primary and secondary oscillations and whose respective locations are in close agreement with

$$(m \times f_e) + (n \times f_o) \text{ [Hz]}, \quad (27)$$

where  $m$  and  $n$  are integers in the range  $[-\infty \dots -3, -2, -1, 0, 1, 2, 3, \dots \infty]$ .

In the manner of Fig. 6, the presented model was observed to predict the frequency of the two strongest oscillations in accordance with Eqs. (4) and (25) for various

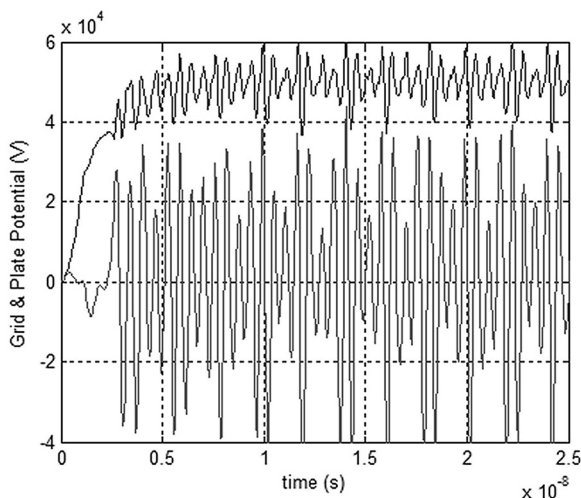


FIG. 5. Calculated grid potential  $V_g$  (upper) and plate potential  $V_p$  (lower) as a function of time.  $V_s(0) = 50$  kV and  $L_{pc} = 10$  nH.

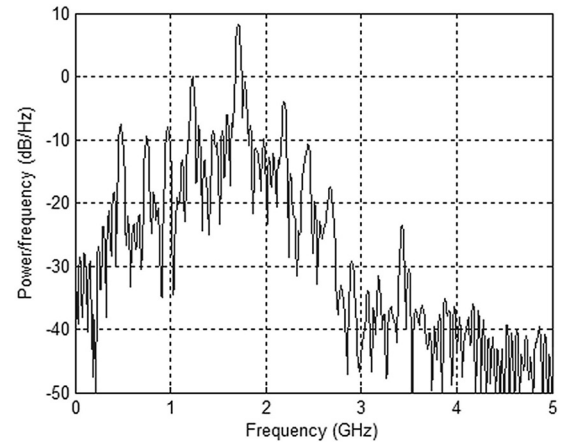


FIG. 6. Estimated power spectral density.  $L_{pc} = 10$  nH and  $V_s(0) = 50$  kV.

electrode dimensions and operating voltages input to the model, provided the cavity inductance  $L_{pc}$  was chosen such that  $f_e \neq f_o$ . For any given set of electrode dimensions and single operating potential input to the model, the two dominant oscillations were observed to move closer to each other as the cavity inductance was adjusted, such that the cavity resonant frequency  $f_o$  approached the electron frequency  $f_e$ . However, at such point as the two merged, the frequency of the resultant single oscillation would increase by a factor of 1.2. The exact cause of this is not known but is suspected to be due to the sympathetic action of the grid potential upon electrons reflexing about the grid, in much the same way as the plate potential acts upon the virtual cathode.

Fig. 7 shows the calculated grid and plate potentials over a period of 25 ns for the case of the same dimension electrodes as Fig. 5, but with  $L_{pc} = 3.8$  nH such that  $f_e = f_o$ , that is to say, the VCO is operated in resonance.

An estimation of the power spectral density of the data of Fig. 7 between 10 ns and 25 ns, determined following the periodogram method, is shown in Fig. 8. As anticipated, a single peak is visible, indicating oscillation at a single frequency, as would be expected of a microwave tube operated at resonance. As described above, however, the frequency of

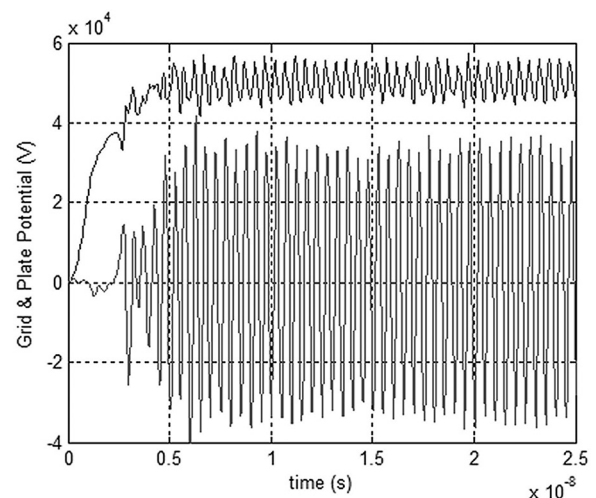


FIG. 7. Grid potential  $V_g$  (upper) and plate potential  $V_p$  (lower) as a function of time.  $V_s(0) = 50$  kV and  $L_{pc} = 3.8$  nH.



the single oscillation has risen to  $\sim 2$  GHz, which is a factor of 1.2 greater than the value of 1.66 GHz predicted by Eq. (4).

## VI. EFFICIENCY

The presented model may be usefully employed to predict the efficiency of the VCO (both in and out of resonance) by comparing the average input power  $P_{in(av)}$  with the average output power  $P_{out(av)}$ , where

$$P_{in(av)} = \frac{1}{T} \int_0^T V_{gc} I_g dt \quad [\text{W}] \quad (28)$$

and

$$P_{out(av)} = \frac{1}{T} \int_0^T \frac{V_{pc}^2}{R_{pc}} dt \quad [\text{W}]. \quad (29)$$

The duration  $T$  over which this average was determined was typically set to  $\sim 4$  ns to encompass at least 4 to 5 oscillations, and the model set to simulate at least 100 ns of operation. Equations (28) and (29) were implemented repeatedly (cycling every  $T$  seconds) in order to determine a running average.

With  $V_s(0) = 50$  kV and  $L_o = 3.8$  nH,  $P_{in(av)}$  and  $P_{out(av)}$  settled (after the initial onset of oscillation) to values of 45 MW and 15 MW, respectively, indicating a predicted conversion efficiency of  $\sim 33\%$  at resonance. At a mean grid potential of 50 kV, the VCO has a predicted input impedance of  $\sim 55 \Omega$ , determined by dividing the mean grid potential by the grid current. The input impedance is real over the time frame of interest, during which time the grid potential and grid current both remain reasonably constant. With  $L_{pc} = 10$  nH (marginally out of resonance),  $P_{in(av)}$  and  $P_{out(av)}$  dropped to 44 MW and 11 MW, respectively, indicating a reduced conversion efficiency of  $\sim 25\%$ . With the plate disconnected from the cathode (significantly out of resonance)  $P_{in(av)}$  and  $P_{out(av)}$  dropped to 41 MW and 4 MW, respectively, indicating a significantly reduced conversion efficiency of only  $\sim 10\%$ . The model thus serves to illustrate

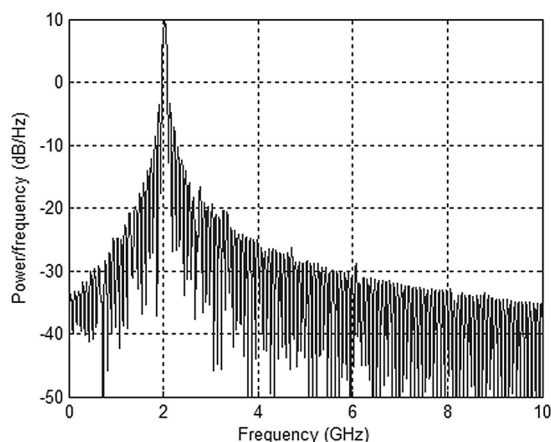


FIG. 8. Power spectral density.  $L_{pc} = 3.8$  nH and  $V_s(0) = 50$  kV.

that the maximum conversion efficiency is achieved, as would be expected, when the VCO is operated in resonance. Calculated values are similar to the values quoted by Didenko for his VCO.<sup>9</sup>

## VII. CONCLUSIONS

A one-dimensional electrostatic model of a relativistic coaxial geometry VCO with centrally located cathode and peripherally located plate has been presented. The model predicts the formation and movement of a virtual cathode for a space-charge limited current of electrons through the cavity. A Fourier transform of the plate-cathode potential indicates oscillation at frequencies in reasonable agreement with those predicted by Eqs. (4) and (25), provided the VCO is operated out of resonance. As resonance is approached, the model predicts that the frequency of the single resultant oscillation will increase by a factor of 1.2. The model further predicts the enhanced emission of microwave radiation when operated at resonance, with a transfer efficiency of  $\sim 33\%$  considered to be possible provided an acceptable impedance match can be achieved between the VCO and the attached waveguide.

One distinct disadvantage of the presented model is that it is *electrostatic* only, and not *electromagnetic*. Ergo, the model is not expected to predict the precise behavior of the presented VCO, but is still considered a useful tool for understanding the mechanism of virtual cathode formation and the reflexing of electrons about the grid. Greater accuracy, at the expense of model run-time, is anticipated for the case of a fully electromagnetic model, with which it would be possible to discard the cavity inductance and load in favour of a model able to predict the magnetic flux coupled to the inter-electrode space as a function of the electrode and wave-guide geometry, as well as examine the propagation of the resultant EM wave down a finite length of waveguide. A fully electromagnetic model is under consideration as a future advancement of the presented work.

<sup>1</sup>M. Crawford, M. Kristiansen, and L. Hatfield, in *10th IEEE International Pulsed Power Conference on Digest of Technical Papers, Albuquerque, NM* (IEEE, 1995), p. 682.

<sup>2</sup>W. Jiang, K. Woolverton, J. Dickens, and M. Kristiansen, *IEEE Trans. Plasma Sci.* **27**(5), 1538 (1999).

<sup>3</sup>W. Jiang, J. Dickens, and M. Kristiansen, *IEEE Trans. Plasma Sci.* **27**(5), 1543 (1999).

<sup>4</sup>C. K. Birdsall and W. B. Bridges, *J. Appl. Phys.* **32**(12), 2611 (1961).

<sup>5</sup>V. L. Granatstein, P. Sprangle, R. K. Parker, and M. Herndon, *J. Appl. Phys.* **46**(5), 2021 (1975).

<sup>6</sup>R. A. Mahaffey, P. Sprangle, J. Golden, and C. A. Kapetanacos, *Phys. Rev. Lett.* **39**(13), 843 (1977).

<sup>7</sup>H. E. Brandt, A. Bromborsky, H. B. Bruns, and R. A. Kehs, in *2nd International Topical Conference on Electron Beam Research & Technology, Ithaca, NY* (IEEE, 1977), p. 649.

<sup>8</sup>D. A. Phelps, *IEEE Trans. Plasma Sci.* **6**(1), 76 (1978).

<sup>9</sup>A. N. Didenko, A. G. Gerlitsin, V. I. Zelnetsov, G. P. Fomenko, Yu. G. Shtein, and G. Yushkov, in *International Topical Conference on Electron Beam Research and Technology, Albuquerque, NM* (IEEE, 1975), p. 424.

<sup>10</sup>A. G. Zherlitsyn, S. I. Kuznetsov, G. V. Melnikov, G. P. Fomenko, and V. I. Tsvetkov, *Sov. Tech. Phys. Lett.* **11**(9), 450 (1985).

<sup>11</sup>D. J. Sullivan, J. E. Walsh, and E. A. Coutsias, "Virtual cathode oscillator theory," in *High Power Microwave Sources*, edited by V. L. Granatstein and I. A. Alexeff (Artech House, 1987), p. 441.

- <sup>12</sup>L. E. Thode, "Virtual-cathode microwave device research: Experiment and simulation," in *High Power Microwave Sources*, edited by V. L. Granatstein and I. A. Alexeff (Artech House, 1987), p. 507.
- <sup>13</sup>R. F. Hoeberling and M. V. Fazio, *IEEE Trans. Electromagn. Compat.* **34**(3), 252 (1992).
- <sup>14</sup>J. Benford, J. A. Swegle, and E. Schamiloglu, *High Power Microwaves* (Taylor & Francis, 2007), p. 435.
- <sup>15</sup>E. H. Choi, K. Y. Sung, W. Jeon, J. Jung, J. G. Kim, and Y. Seo, *J. Korean Phys. Soc.* **44**(5), 1049 (2004).
- <sup>16</sup>X. Luo, C. Liao, and F.-B. Meng, in *7th International Symposium on Antennas, Propagation and EM Theory, Guilin, China* (IEEE, 2006), p. 1.
- <sup>17</sup>D. Biswas and R. Kumar, *IEEE Trans. Plasma Sci.* **38**(6), 1313 (2010).
- <sup>18</sup>D. Biswas and R. Kumar, in *IEEE International Vacuum Electronics Conference, Bangalore, India* (IEEE, 2011), p. 171.
- <sup>19</sup>D. J. Wootton, J. A. Lucken, and R. C. Bannerman, *Proc. IEE, Part B* **105**(12), 969 (1958).
- <sup>20</sup>M. V. Fazio, B. L. Freeman, R. F. Hoeberling, J. Kinross-Wright, D. G. Rickel, and R. M. Stringfield, *IEEE Trans. Plasma Sci.* **20**(3), 305 (1992).
- <sup>21</sup>R. B. Miller, *J. Appl. Phys.* **84**(7), 3880 (1998).
- <sup>22</sup>E. Garate, R. D. McWilliams, D. E. Voss, A. L. Lovesee, K. J. Hendricks, T. A. Spencer, M. Collins Clark, and A. Fisher, *Rev. Sci. Instrum.* **66**(3), 2528 (1995).
- <sup>23</sup>D. Shiffler, M. Ruebush, M. Haworth, R. Umstaddt, M. LaCour, K. Golby, D. Zagar, and T. Knowles, *Rev. Sci. Instrum.* **73**(12), 4358 (2002).
- <sup>24</sup>R. Prohaska and A. Fisher, *Rev. Sci. Instrum.* **53**(7), 1092 (1982).
- <sup>25</sup>F. F. Rieke, "The space charge as a circuit element," in *Microwave Magnetrons*, edited by G. B. Collins (McGraw-Hill, 1948), p. 305.